

Flexural behavior of concrete beams reinforced with different types of fibers

Hind M. Kh.^{*1}, Mustafa Özakça^{1a}, Talha Ekmekyapar^{1b} and Abdolbaqi M. Kh.^{2c}

¹Department of Civil Engineering, University of Gaziantep, 27310 Gaziantep, Turkey

²Faculty of Mechanical Engineering, University Malaysia Pahang, 2600 Pekan, Pahang, Malaysia

(Received June 10, 2016, Revised July 29, 2016, Accepted September 12, 2016)

Abstract. Enhanced tensile properties of fiber reinforced concrete make it suitable for strengthening of reinforced concrete elements due to their superior corrosion resistance and high tensile strength properties. Recently, the use of fibers as strengthening material has increased motivating the development of numerical tools for the design of this type of intervention technique. This paper presents numerical analysis results carried out on a set of concrete beams reinforced with short fibers. To this purpose, a database of experimental results was collected from an available literature. A reliable and simple three-dimensional Finite Element (FE) model was defined. The linear and nonlinear behavior of all materials was adequately modeled by employing appropriate constitutive laws in the numerical simulations. To simulate the fiber reinforced concrete cracking tensile behavior an approach grounded on the solid basis of micromechanics was used. The results reveal that the developed models can accurately capture the performance and predict the load-carrying capacity of such reinforced concrete members. Furthermore, a parametric study is conducted using the validated models to investigate the effect of fiber material type, fiber volume fraction, and concrete compressive strength on the performance of concrete beams.

Keywords: finite element modeling; reinforced concrete; synthetic fibers; mineral fibers; steel fibers

1. Introduction

Nowadays, increasing the use of supplementary cementitious materials in concrete is a common approach to reduce carbon emissions. Supplementary cementitious materials, such as ground granulated blast-furnace slag and fly ash, as well as fiber and polymer modification, have been widely used in concrete to improve its workability and long-term performance (Yu *et al.* 2016). Fiber reinforced concrete is also widely used in many civil engineering applications (e.g. industrial pavements, tunnel linings, marine structures, earthquake-resistant structures, etc.) (Radi *et al.* 2015).

*Corresponding author, Ph.D., E-mail: hindmahmood18@gmail.com

^aProfessor, E-mail: ozakca@gantep.edu.tr

^bAsstant Professor, E-mail: ekmekyapar@gantep.edu.tr

^cPh.D., E-mail: abdolbaqi.mk@gmail.com

Several researchers have investigated the effects of fiber inclusion in cement matrix depending on the fiber content and type to improve the mechanical and fracture properties (Yoo, Yoon *et al.* 2015). Fiber inclusion in the matrix greatly influences the properties of concrete and various studies have shown that the fibers can significantly enhance the engineering properties of the concrete such as the flexural strength, tensile strength, fatigue and abrasion resistance, impact, toughness, load bearing capacity after cracking and deformation capability (Monteiro 2006, Jiang, Fan *et al.* 2014). It's always difficult to identify the effects of fibers on the properties of concrete due to the extreme heterogeneity of concrete. However, the actual fiber that must be used depends mainly on the application needed for the concrete. These fibers may be distinguished by their different chemical or physical properties, such as the fiber's nature (synthetic, mineral or steel), their mechanical properties, and its geometry (macro fiber vs. micro fiber), as their aspect ratio (L/ϕ), etc. (Hannawi, Bian *et al.* 2016).

In general, these different properties of fiber yield different effects when added to their respective concretes. Ivan (Markovic 2006) observed that the micro fiber (shorter than 0.1 mm) has a more homogenous distribution in concrete, leading to a higher packing density of the cement matrix. Keer (Marshall 1992) indicated that synthetic fiber increases the permeability of concrete due to their porous interfacial transition zone (ITZ). As far as the mechanical performances of concrete are concerned, many researchers (Li 1998, Lu and Hsu 2006, Nguyen, Ryu *et al.* 2014, Wille, El-Tawil *et al.* 2014) have investigated the fibers' effect on concrete under tension or compression. They have found that the fibers increase the tensile strength of concrete, but not necessarily its compressive strength. They have also reported that the macro fiber has an efficacious capacity against the macro cracking of concrete in the post-peak phase. (Nataraja, Dhang *et al.* 1999) indicated that fibers yield a higher compressive strength in the concrete with a greater ratio of (L/ϕ). Zheng (Zheng and Feldman 1995) showed that fibers with higher elastic modulus and higher tensile strength could significantly improve the mechanical performance of concrete.

T. S. Nagaraj and H. V. Dwarakanath (Nagaraj and Dwarakanath 1984) conducted experimental and analytical studies on steel fiber reinforced concrete beam with the different volume fractions of fiber (1%, 2%, 3%). They reported that the flexural strength of the reinforced concrete beam increased with an increase in the steel fiber (SF) volume fraction irrespective of the fiber length or mix composition. The flexural toughness, shear toughness, and compression toughness index of the reinforced concrete beam showed a considerable increase with an increase in the fiber content which was true regardless of the fiber length or type of matrix. Jun Zhang *et al.* (Zhang, Wang *et al.* 2014) numerically and experimentally investigated the flexural behavior of engineered cementitious composite beams reinforced with 2% volume fraction of PVA fiber. The authors observed that the use of a PVA fiber in reinforcing concrete beams would achieve desirable strength and ductility limits.

It appears from the aforementioned investigations that numerous finite element models have been developed to simulate the behavior of reinforced concrete beams (Maalej and Leong 2005, Yuan, Pan *et al.* 2014, Hawileh 2015, Bencardino, Condello *et al.* 2016). However, limited finite element models had been conducted on simulating the response of concrete beams reinforced with short fibers (Maalej and Leong 2005, Yuan, Pan *et al.* 2014). The main aim of this study is to develop a finite element (FE) model that can capture the effect of different types of fibers with different volume fractions on the flexural capacity of concrete beams. Therefore, the current study involves a development of FE models that can accurately predict the response of concrete beams reinforced with synthetic, mineral, and steel fibers. The developed FE models were validated by

comparing the numerical results with some experimental data available in literature (Nagaraj and Dwarakanath 1984, Zhang, Wang *et al.* 2014). Moreover, these FE models captured the behavior and predicted the deflection, crack patterns, and ultimate load carrying capacity of the tested specimens with a high level of accuracy. This allows to evaluate numerically the behavior of similar fiber reinforced concrete beams, subjected to increase a static load up to failure, without having to measure experimentally. In addition, a parametric study was carried out to investigate the effect of fiber material type, fiber volume fraction, and concrete compressive strength on the flexural performance of fiber reinforced concrete beams.

2. Experimental data

In order to assess the capability of the proposed FE model, a comparison between numerical results and experimental data was conducted to predict the overall structural behavior of fiber reinforced concrete beams in terms of load-midspan deflection curves, ultimate load values, and crack patterns at failure. Therefore, the following two experimental studies have been considered to provide measures concerning all comparison parameters, as well as the geometry of the beams and the mechanical properties of the materials:

- T. S. Nagaraj and H. V. Dwarakanath (Nagaraj and Dwarakanath 1984) carried out experimental investigation of two concrete beams ($100 \times 100 \times 500$ mm): one reinforced with steel fiber (SF) of 1% volume fraction, and one with steel fiber of 3% volume fraction. The reinforced concrete beam specimens were tested at loading condition of 28-day testing age under four points bending gradually to failure as illustrated in Fig.1.

- Jun Zhang *et al.* (Zhang, Wang *et al.* 2014) investigated the flexural performance of cementitious composite beam ($100 \times 100 \times 400$ mm) contains about 2% of PVA fibers. The results of the reinforced beam were compared with the plain concrete (reference beam) results. The beams were tested under three-point bending load and loading condition of 28-day testing age. More details about the tested beams are shown in Fig. 2.

A total number of four experimental results were collected. The mechanical properties of the materials are summarized in Table 1, where for each experimental work are given: specimen name, compressive strength (f'_c), modulus of elasticity ($E_{con.}$), and tensile strength (f_t) of the concrete, length (L), diameter (ϕ), density (ρ), ultimate strength (f_{fu}), and elastic modulus (E_f) of the fibers.

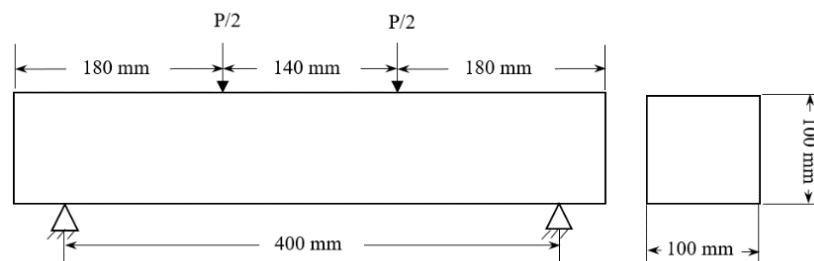


Fig. 1 Geometrical properties of the beam tested by T. S. Nagaraj and H. V. Dwarakanath (Nagaraj and Dwarakanath 1984)

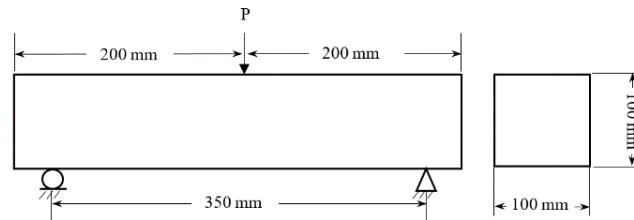
Fig. 2 Geometrical properties of the beam tested by Jun Zhang *et al.* (Zhang, Wang *et al.* 2014)

Table 1 Mechanical properties of the beams

Experimental work	Specimen name	f_c (MPa)	E_{con} (GPa)	f_t (MPa)	L (mm)	ϕ (μm)	ρ_f (kg/m^3)	f_{fu} (GPa)	E_f (GPa)
T. S. Nagaraj and H. V. Dwarakanath (Nagaraj and Dwarakanath 1984)	EXP (SF 1.0%)	30	25	3.5	36	500	7800	1-3	200
	EXP (SF 3.0%)	30	25	3.5	36	500	7800	1-3	200
Jun Zhang <i>et al.</i> (Zhang, Wang <i>et al.</i> 2014)	EXP (PC)	30	25	3.5	-----	-----	-----	-----	-----
	EXP (PVA 2%)	30	25	3.5	12	39	1300	1.62	42.8

Table 2 Designation of the tested specimens (Nagaraj and Dwarakanath 1984, Zhang, Wang *et al.* 2014) and corresponding FE models

Specimen	FE model
EXP (SF 1.0%)	FE (SF 1.0%)
EXP (SF 3.0%)	FE (SF 3.0%)
EXP (PC)	FE (PC)
EXP (PVA 2.0%)	FE (PVA 2.0%)

3. FE Modeling

3.1 Geometrical modeling

The numerical analysis was conducted using the FE software ANSYS 15.0 (2015) to develop 3D FE models of the specimens tested by T. S. Nagaraj and H. V. Dwarakanath (Nagaraj and Dwarakanath 1984) and Jun Zhang *et al.* (Zhang, Wang *et al.* 2014). The designation of the tested specimens and the corresponding FE models are given in Table 2. The properties of the constituent materials, geometry, static loading, and boundary conditions in the developed FE models are similar to the tested specimens.

All the tested beams were modelled using brick SOLID65 (2015) elements to model nonlinear behavior of fiber reinforced concrete. The brick SOLID65 is an eight noded element with three translational degrees of freedom (*dof*) per node, and the element has the capability of cracking in tension and crushing in compression. The loading and rigid steel supports are modeled using the brick SOLID45 (2015) elements with elastic steel material properties to avoid any major stress concentration problems on the concrete material at those specified locations that will lead to divergence in the solution. The SOLID45 element has the same properties as that of SOLID65 except for the capability of cracking in tension and crushing in compression.

3.2 Materials models

3.2.1 Fiber reinforced concrete

In order to model the crack propagation in fiber reinforced concrete beams, the approach grounded on the solid basis of micromechanics developed by Tetsushi Kanda *et al.* (Kanda, Lin *et al.* 2000) is used in this study. This model provides simple analytic formulas for the stress-strain relation of pseudo-strain hardening cementitious composite. The assumption of this approach is that fibers are uniformly distributed in the matrix and the fiber reinforced concrete beams is thus modeled as a homogeneous material. It assumes that the main two failure mechanisms are tensile cracking and compressive crushing of the concrete and it allows the definition of strain hardening in compression and strain softening (or stiffening) in tension. In the linear elastic range the behavior was defined by the elastic modulus (E_c) and Poisson's ratio (ν_c) which calculated by Eq. (1) and Eq. (2) (Daniel, Ishai *et al.* 1994)

$$E_c = V_f E_f + V_m E_m \quad (1)$$

$$\nu_c = V_f \nu_f + V_m \nu_m \quad (2)$$

Where: E_c , E_f , and E_m are the modulus of elasticity of composite, fiber, and matrix, respectively. ν_c , ν_f , and ν_m are Poisson's ratio of composite, fiber, and matrix, respectively.

In the plastic range the stress-strain curves for strain hardening (Fig. 3) and strain softening (Fig. 4) were requested. The hardening behavior was modeled based on stress-strain relation and the softening behavior was modeled based on stress-crack opening displacement (COD) relation. It must be noted that the stress-COD relation should be used after the ultimate state (Kanda, Lin *et al.* 2000). The relations were defined as follow (Kanda, Lin *et al.* 2000):

$$\sigma(\varepsilon) = \begin{cases} E_c \varepsilon & \varepsilon \leq \sigma_{ss} / E_c \\ \sigma_i + E_{ie} \varepsilon & \varepsilon > \sigma_{ss} / E_c \end{cases} \quad (3)$$

Where

$$E_{ie} = \left(\frac{\sigma_{peak} - \sigma_{ss}}{\varepsilon_{cu} - \sigma_{ss} / E_c} \right); \quad \sigma_i = \sigma_{ss} \left(1 - \frac{E_{ie}}{E_c} \right)$$

ε_{cu} is the ultimate strain, σ_{ss} is the steady-state cracking stress, σ_{peak} is the ultimate stress, and E_c is the composite elastic modulus.

$$\frac{\hat{\sigma}_c}{g} = \sqrt{2\bar{c}} - \frac{\bar{c}}{2} \quad (4)$$

$$\frac{\hat{\sigma}_{fc}}{g} = \left(\frac{2\sqrt{2}}{3} \sqrt{\bar{c}} - \frac{\bar{c}}{4} \right) + \frac{\sqrt{\pi}}{2\bar{c}} \bar{K} \quad (5)$$

Where

$$\hat{\sigma}_{fc} = \frac{\sigma_{fc}}{\sigma_0}; \quad \hat{\sigma}_c = \frac{\sigma_c}{\sigma_0}; \quad \sigma_0 = \frac{V_f \tau_i}{2} \left(\frac{L_f}{d_f} \right); \quad g = \frac{2}{4 + f^2} (1 + e^{f^2/2})$$

σ_c is the composite crack bridging stress, σ_{fc} is the stress level at which each of the multiple cracks propagates, when each crack at a different part of the specimen has a different size, f is the

snubbing coefficient, τ_i is the frictional bond strength, V_f is the fiber volume fraction, L_f is the fiber length, and d_f is the fiber diameter.

$$\bar{c} = \frac{\sqrt{\hat{c}}}{\hat{\delta}^*}; \quad \hat{c} = \frac{c}{c_i}; \quad \hat{\delta}^* = \frac{2\tau}{E_f(1+\eta)} \frac{L_f}{d_f}; \quad \eta = \frac{V_f E_f}{V_m E_m}; \quad \bar{K} = \frac{K_{tip}}{\sigma_0 \sqrt{c_i}} \frac{1}{g \hat{\delta}^*};$$

$$c_i = \left(\frac{L_f E_c}{2K_{tip}} \right)^2 \frac{\pi}{16(1-\nu^2)^2}; \quad K_{tip} = \frac{E_c}{E_m} K_m; \quad V_m = 1 - V_f$$

c is the flaw radius, E_f is the fiber elastic modulus, V_m is the matrix volume fraction of matrix, E_m is the elastic modulus of matrix; K_{tip} is the crack tip fracture toughness, E_c is the elastic modulus of composite; ν is the Poisson's ratio of composite, and K_m is the matrix fracture toughness.

$$\hat{\sigma}_{ss} = g \left(\sqrt{2\bar{c}_s} - \frac{\bar{c}_s}{2} \right) \quad (6)$$

Where

$$\hat{\sigma}_{ss} = \frac{\sigma_{ss}}{\sigma_0}; \quad \bar{c}_s = \frac{\sqrt{\hat{c}_s}}{\hat{\delta}^*}; \quad \hat{c}_s = \frac{c_s}{c_i}$$

The term \bar{c}_s is the flaw size as steady-state cracking occurs and is determined by solving Eq. (7)

$$\frac{2}{\sqrt{\pi}} \bar{c}_s \left(\frac{\sqrt{2\bar{c}_s}}{3} - \frac{\bar{c}_s}{4} \right) = \bar{K} \quad (7)$$

$$\sigma_{peak} = g \sigma_0 \quad (8)$$

$$\varepsilon_{cu} = \frac{\delta_{peak}}{x_d^{theory}} \quad (9)$$

Where δ_{peak} is the ultimate COD, and x_d^{theory} is the theoretically predicted ultimate crack spacing.

$$\delta_{peak} = \frac{b - \sqrt{b^2 - 4a}}{2} \quad (10)$$

Where

$$b = \frac{2a_2 - 3a_1}{4a_2}; \quad a = \frac{a_1 - 2}{4a_2}; \quad a_1 = \frac{\beta_1 L_f}{2d_f}; \quad a_2 = \frac{\beta_2 L_f^2}{4d_f^2}$$

β_1 is the first-order nondimensional hardening parameter; and β_2 is the second-order nondimensional hardening parameter. The parameters β_1 and β_2 are phenomenological (interface) parameters determined from the load-displacement relation obtained in the pull-out test of a single fiber embedded in the matrix.

$$x_d = \frac{L_f - \sqrt{L_f^2 - 2\pi\psi L_f x}}{2} \quad (11)$$

Where
$$\psi = \frac{4}{\pi g}; \quad x = \frac{V_m \sigma_{mu} d_f}{4V_f \tau_i}$$

Where σ_{mu} is the tensile strength of matrix.

The distribution of flaw size can be treated as a random process and expressed by the Weibull-type function (Weibull 1951)

$$F(\bar{c}) = \exp\left[-\frac{1}{\lambda} \left(\frac{\bar{c}_0}{\bar{c}}\right)^m\right] \tag{12}$$

Where λ is the scale factor, m is the Weibull modulus, and \bar{c}_0 is the reference crack radius.

$$x_d^{theory} = \frac{x_d}{1 - F(\bar{c}_{mc})} \tag{13}$$

$x_d^{theory} = x_d$ if all flaws are of size larger than c_{mc} , when $F = 0$, corresponding to the fully saturated case. When some flaws are of a size less than c_{mc} , the case of unsaturated multiple cracking prevails (Kanda, Lin *et al.* 2000).

3.2.2 Plain concrete

In order to model the nonlinear behavior of the plain concrete (reference beam), the compressive and tensile stress-strain relationships should be defined. The employed constitutive concrete material model is based on the theory of William and Warnke (Willam and Warnke 1975) model, which requires the following five input strength parameters

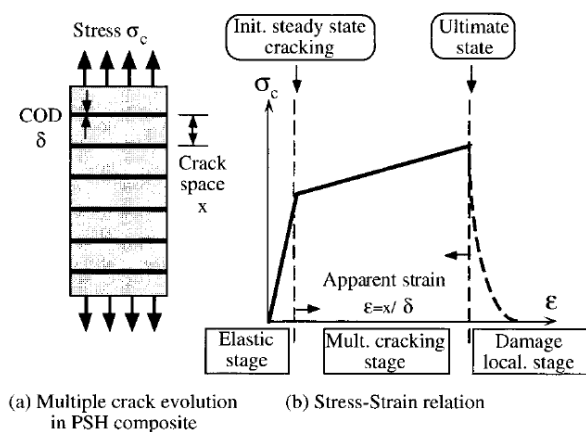


Fig. 3 Tensile behavior representation for pseudo strain hardening composites

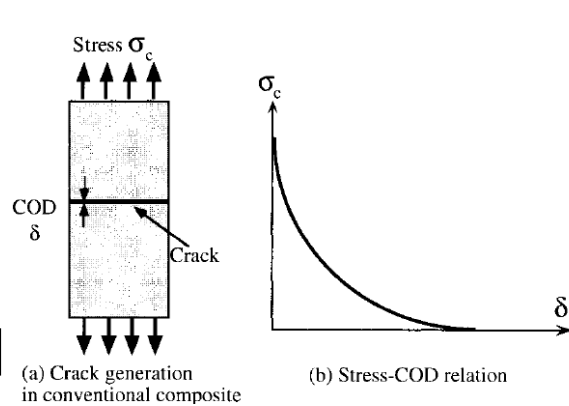


Fig. 4 Tensile behavior representation for conventional strain hardening composites

uniaxial tensile strength (f_t), uniaxial compressive strength (f'_c), biaxial compressive strength (f_{cb}), compressive strength for a state of biaxial compression superimposed on hydrostatic stress

state (f_1), and uniaxial compression superimposed on hydrostatic stress state (f_2). The adopted values for f_t and f_c' are taken from the obtained experimental data shown in Table 1. The other three parameters, f_{cb} , f_1 , and f_2 default to William and Warnke (William and Warnke 1975) and were taken as $1.2 f_c'$, $1.45 f_c'$, and $1.725 f_c'$, respectively. It should be noted that the adopted parameters are within the range used in the available literature (Hawileh, El-Maaddawy *et al.* 2012, Hawileh, Naser *et al.* 2013, Manos, Theofanous *et al.* 2014).

According to the William and Warnke model (William and Warnke 1975), the concrete element in tension will crack and lose stiffness upon reaching its tensile strength. Therefore, the behavior of the concrete element in tension was modeled as linear elastic up to the concrete tensile strength (William and Warnke 1975, 2015). The stress relaxation in tension is represented by a step drop in the concrete tensile stress by 40%, beyond which the curve descends linearly to zero tensile stress at a strain value six times larger than strain value at the concrete's tensile strength (William and Warnke 1975, 2015). The William and Warnke model (2015) also requires values for the open and closed shear coefficients, that were taken as 0.3 and 0.5, respectively (Hawileh, El-Maaddawy *et al.* 2012, Hawileh, Naser *et al.* 2013). The concrete compressive behavior was modeled with the well-known stress-strain relationship proposed by Hognestad (Hognestad, Hanson *et al.* 1955)

$$f_c = f_c' \left[2 \left(\frac{\varepsilon}{\varepsilon_o} \right) - \left(\frac{\varepsilon}{\varepsilon_o} \right)^2 \right] \quad (14)$$

where f_c is the compressive stress in the concrete (MPa) corresponding to the specified strain ε , f_c' is the concrete compressive strength (Table 1) and ε_o is the peak compressive strain equal to $2f_c' / E_{con}$.

3.3 Solution technique, mesh and convergence issues

In the nonlinear analysis, the total load applied to finite element model is divided into a series of load increments called load steps. At the completion of each incremental solution, the stiffness matrix of the model is adjusted to reflect nonlinear changes in structural stiffness before proceeding to the next load increment. The Newton–Raphson equilibrium iterations for updating the model stiffness were used in the nonlinear solutions.

In this study, convergence criteria for the FE models were based on force and displacement, and the convergence tolerance limits were initially selected by analysis program, which was 0.001. For the nonlinear analysis, automatic time stepping through the ANSYS program predicts and controls load step sizes. Based on the previous solution history and the physics of the models, if the convergence behavior is smooth, automatic time stepping will increase the load increment up to a selected maximum load step size. If the convergence behavior is abrupt, automatic time stepping will bisect the load increment until it is equal to a selected minimum load step size. The maximum and minimum load step sizes are required for the automatic time stepping.

Mesh convergence study with three fine mesh sizes, 15mm, 10mm, and 5mm were carried out. It was found that the result obtained from a 10 mm mesh size beam was more accurate. Further refinements presented same results as the previous mesh but consuming more time for computations. Thus, a 10×10×10mm mesh size was finally chosen for all FE models. The solution

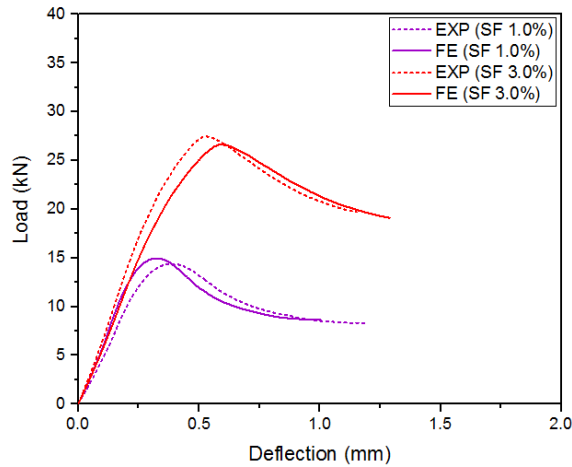


Fig. 5 Numerical load-mid span deflection curves versus test results of T. S. Nagaraj and H. V. Dwarakanath (Nagaraj and Dwarakanath 1984)

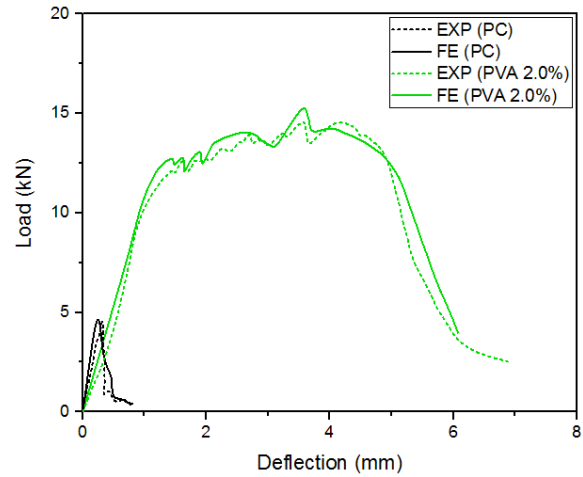


Fig. 6 Numerical load-mid span deflection curve versus test results of Jun Zhang *et al.* (Zhang, Wang *et al.* 2014)

Table 3 Experimental and FE results

Specimen	FE model	Ultimate load (kN)		Difference (P_{EXP}/P_{FE}) %	Ultimate deflection (mm)		Difference (δ_{EXP}/δ_{FE}) %
		P_{EXP}	P_{FE}		δ_{EXP}	δ_{FE}	
EXP (SF 1.0%)	FE (SF 1.0%)	15.20	15.60	2.56%	0.38	0.35	-8.57%
EXP (SF 3.0%)	FE (SF 3.0%)	28.60	28.10	-1.78%	0.55	0.57	3.51%
EXP (PC)	FE (PC)	4.73	4.55	-3.96%	0.32	0.30	-6.67%
EXP (PVA 2.0%)	FE (PVA 2.0%)	14.71	14.92	1.41%	4.18	3.87	-8.01%

time with this mesh was approximately 3-4 h using processor Intel(R) Core(TM) i7-3930K (3.20 GHz).

3.4 Numerical results

The numerical results in terms of load-midspan deflection curves have been illustrated in Figs. 5 and 6 for all the analyzed beams. The beams reinforced with steel fiber failed in ductile flexure followed by concrete crushing at the midspan section as shown in Fig. 5. In contrast, the beam reinforced with PVA fiber did not fail by concrete crushing, but achieved the ultimate stage by rupture of the PVA fiber. Fig. 6 highlights these numerical results.

Furthermore, Table 3 presents the numerical and experimental results for the load-carrying capacity and deflection at failure. The most obvious finding from Figs. (5, 6) and Table 3 is that the predicted FE results from the present study agree relatively well with that from the experimental study, with a maximum deviation less than 10%. In conclusion, the developed models in the current study could be used to identify the behavior of concrete beams reinforced with short fibers with reasonable accuracy. In addition, the use of wide range of mechanical properties from the developed FE models can provide designers and researchers with valuable insights into the performance of concrete beams reinforced with short fibers.

Table 4 Description of the fibers used in parametric study

	Steel (SF)	Basalt (BF)	Aramid (AF)	Glass (GF)	PVA
Material	Steel	Mineral	Synthetic	Synthetic	Synthetic
Geometry	Macro	Micro	Micro	Micro	Micro
L (mm)	36	12	12	12	12
ϕ (μm)	500	13	15	13	39
ρ (kg/m^3)	7800	2800	1470	2600	1300
f_{tu} (GPa)	1-3	4.1	5.5	3.4	1.62
E_f (GPa)	200	89	180	77	42.8
ν	0.30	0.23	0.28	0.22	0.42
Reference	(Nagaraj and Dwarakanath 1984)	(Kizilkanat, Kabay <i>et al.</i> 2015)	(Vasiliev and Morozov 2013)	(Kizilkanat, Kabay <i>et al.</i> 2015)	(Zhang, Wang <i>et al.</i> 2014)

4. Parametric study

There are a quite few researches so far on the performance of concrete beams reinforced with different types of fibers. Therefore, a parametric study was designed and conducted in terms of load-midspan deflection curves and crack patterns of the beams to advance the knowledge in this field and further investigate the effect of different parameters in structural response of similar beams. The variables of the parametric study are fiber reinforcement material type, fiber volume fraction, and concrete compressive strength. This parametric study used specimens tested by Jun Zhang *et al.* (Zhang, Wang *et al.* 2014), and T. S. Nagaraj and H. V. Dwarakanath (Nagaraj and Dwarakanath 1984) and validated by the developed FE model as reference specimens.

4.1 Fiber material type

The effect of replacing the PVA fibers with synthetic: aramid (AF); glass (GF), mineral: basalt (BF), and conventional steel (SF) fibers on the behavior of the specimen EXP (PVA) will be studied. Four additional FE models are developed having the same geometrical properties used in the specimen EXP (PVA), and fiber volume fraction of 2%. The newly developed models are designated as FE (AF), FE (GF), FE (BF), and FE (SF) representing concrete beams reinforced with aramid, glass, basalt fibers, and steel fibers, respectively. The used values of mechanical properties for the fibers in the developed FE are obtained from the available literature (Nagaraj and Dwarakanath 1984, Vasiliev and Morozov 2013, Kizilkanat, Kabay *et al.* 2015) and given in Table 4.

Fig. 7 shows the response of the different concrete beams reinforced with PVA, AF, GF, BF, and SF fibers. The deflection failure and load-carrying capacity of the studied beams are shown in Table 5. The initial slope of the load–deflection curve of the studied beams is quite similar, and represents the concrete contribution to the load-carrying capacity as clarified in Fig. 7. The stress in the reinforcement is utilized to transfer the applied loadings upon concrete cracking. Thus, it can clearly noticeable a change of slope in the load–deflection response of the studied beams with different types of fibers is as illustrated in Fig. 7. Since the stiffness of the fiber material controls such slope, the beam reinforced with AF fiber, FE (AF) achieved the stiffer response compared to the other four beams, as clarified in Fig. 7 and Table 5.

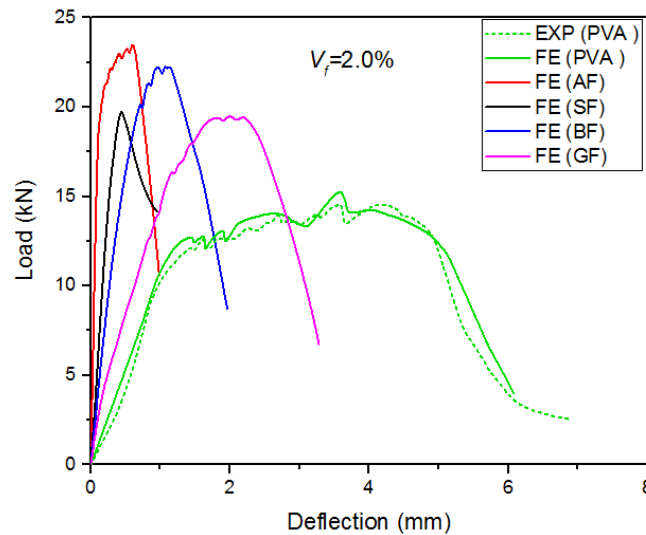


Fig. 7 Effect of fiber material type on the beam's load-mid span deflection response

Table 5 Effect of fiber material type

Specimen	Cracking load (kN)	% Difference (FE/EXP PVA)	Cracking deflection (mm)	% Difference (FE/EXP PVA)	Ultimate load (kN)	% Difference (FE/EXP PVA)	Ultimate deflection (mm)	% Difference (FE/EXP PVA)	Failure deflection (mm)	% Difference (FE/EXP PVA)
EXP (PVA)	12.52	-----	1.68	-----	14.71	-----	4.18	-----	6.98	-----
FE (AF)	15.45	18.96%	0.11	1427.27%	23.63	37.75%	0.57	-633.33%	1.08	-546.29%
FE (GF)	14.87	15.80%	1.07	-57.01%	19.51	24.60%	2.05	-103.90%	3.36	-107.74%
FE (BF)	14.53	13.83%	0.68	-147.06%	22.42	34.39%	1.14	-266.67%	2.01	-247.26%
FE (SF)	12.65	1.04%	0.09	1766.67%	20.70	28.94%	0.46	-808.69%	1.09	-540.37%

The concrete beam reinforced with steel fiber, FE (SF) failed at a maximum load of 20.7 kN with an associated midspan deflection of 0.46 mm, as shown in Fig. 7. However, the other four beams reinforced with different types of fibers FE (PVA), FE (AF), FE (GF), and FE (BF), were able to withstand significant load levels and displacements at failure. It was observed that the load increased at a very small rate in the second change in slope of FE (SF) compared to the initial slope. This behavior can be explained by the weak adhesion between the steel fibers and the matrix, and by their greatest aspect ratio ($L/\phi = 72$) (Hannawi, Bian *et al.* 2016). After a considerable deflection, where the fibers were no longer capable of sustaining the maximum tensile stress, due to the increase in crack width of the structure, the final changes in slope (descending) of the beam specimens were occurred. Further details of these stages are explained in (Hassan, Jones *et al.* 2012, Mahmud, Yang *et al.* 2013). It is also clear from Fig. 7 and Table 5 that the load-carrying capacity of FE (AF), FE (GF), FE (BF), and FE (SF) specimens were higher than FE (PVA) by (18.96%), (15.80%), (13.83%), and (1.04%) for cracking load, and (37.75%), (24.60%), (34.39%), and (28.94%) for ultimate load, respectively.

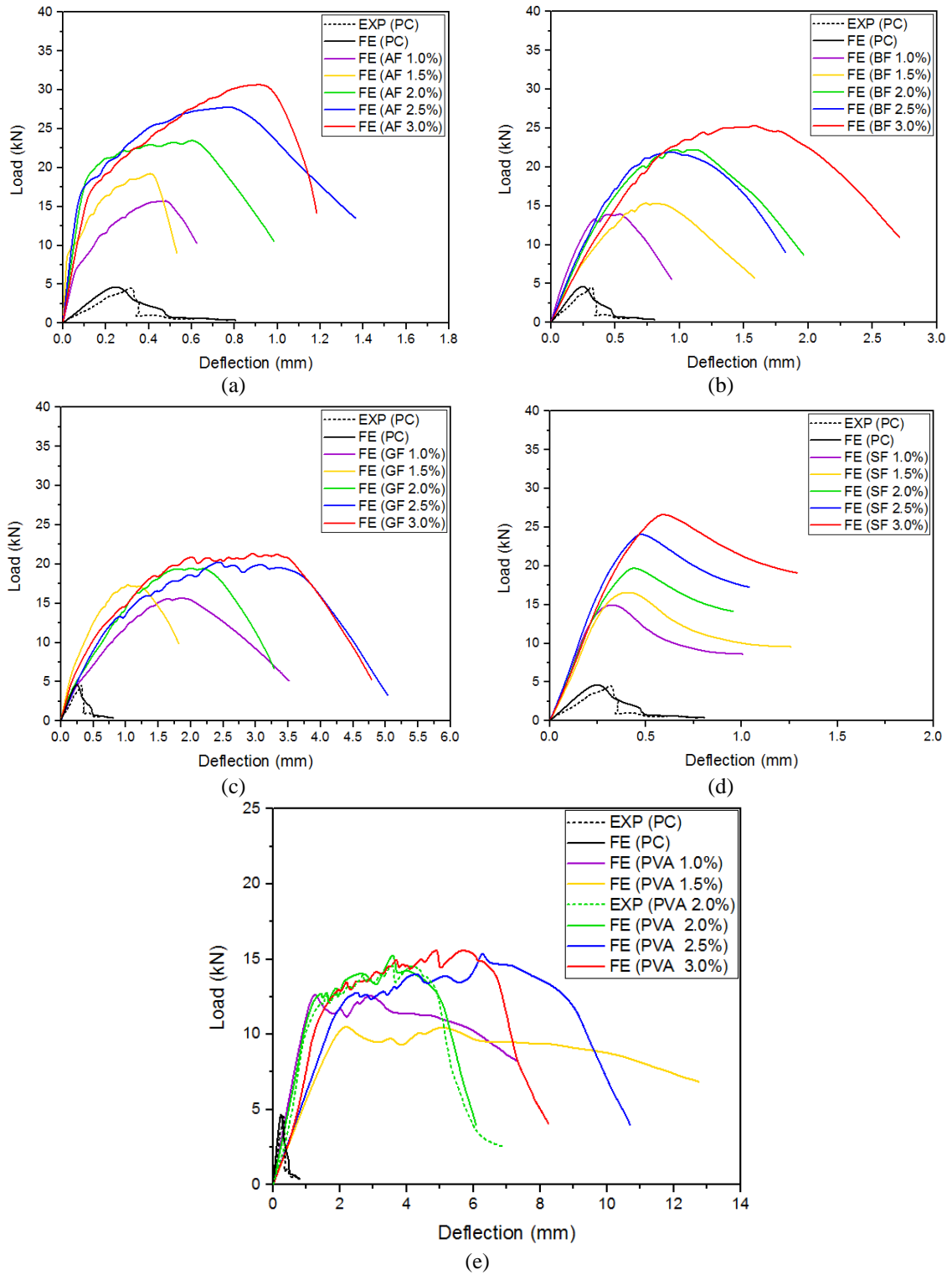


Fig. 8 Effect of fiber volume fraction on the load-mid span deflection response

Table 6 Effect of fiber volume fraction

Specimen	Cracking load (kN)	% Difference (FE/EXP PC)	Cracking deflection (mm)	% Difference (FE/EXP PC)	Ultimate load (kN)	% Difference (FE/EXP PC)	Ultimate deflection (mm)	% Difference (FE/EXP PC)	Failure deflection (mm)	% Difference (FE/EXP PC)
EXP (PC)	2.56	-----	0.07	-----	4.73	-----	0.32	-----	0.86	-----
FE (PVA 1.0%)	10.74	76.16%	0.79	91.14%	13.24	64.27%	1.20	73.33%	7.64	88.74%
FE (PVA 1.5%)	8.75	70.74%	1.49	95.30%	10.98	56.92%	2.10	84.76%	12.88	93.32%
FE (PVA 2.0%)	12.52	79.55%	1.68	95.83%	14.92	68.30%	3.87	91.73%	6.98	87.68%
FE (PVA 2.5%)	13.21	80.62%	4.63	98.49%	14.98	68.42%	6.40	95.00%	10.81	92.04%
FE (PVA 3.0%)	14.06	81.79%	3.98	98.24%	15.76	69.99%	5.73	94.42%	8.40	89.76%
FE (AF 1.0%)	11.87	78.43%	0.34	79.41%	15.71	69.89%	0.48	33.33%	0.65	-32.31%
FE (AF 1.5%)	15.72	83.72%	0.22	68.18%	19.32	75.52%	0.41	21.95%	0.52	-65.38%
FE (AF 2.0%)	15.45	83.43%	0.11	36.36%	23.63	79.98%	0.57	43.86%	1.08	20.37%
FE (AF 2.5%)	23.16	88.95%	0.40	82.50%	27.84	83.01%	0.77	58.44%	1.40	38.57%
FE (AF 3.0%)	26.84	90.46%	0.71	90.14%	30.62	84.55%	0.90	64.44%	1.20	28.33%
FE (GF 1.0%)	13.07	80.41%	1.21	94.21%	15.76	69.99%	1.89	83.07%	3.54	75.71%
FE (GF 1.5%)	14.23	82.01%	0.67	89.55%	17.21	72.52%	1.23	73.98%	1.86	53.76%
FE (GF 2.0%)	14.87	82.78%	1.07	93.46%	19.51	75.76%	2.05	84.39%	3.36	74.40%
FE (GF 2.5%)	17.37	85.26%	1.84	96.19%	20.48	76.90%	2.47	87.04%	5.10	83.14%
FE (GF 3.0%)	18.14	85.89%	1.72	95.93%	21.75	78.25%	2.96	89.19%	4.75	81.89%
FE (BF 1.0%)	10.96	76.64%	0.25	72.00%	14.06	66.36%	0.52	38.46%	0.98	12.24%
FE (BF 1.5%)	11.62	77.97%	0.51	86.27%	15.39	69.27%	0.76	57.89%	1.64	47.56%
FE (BF 2.0%)	14.53	82.38%	0.68	89.71%	22.42	78.90%	1.14	71.93%	2.01	57.21%
FE (BF 2.5%)	17.04	84.98%	0.65	89.23%	21.84	78.34%	0.92	65.22%	1.82	52.75%
FE (BF 3.0%)	20.71	87.64%	0.92	92.39%	25.43	81.40%	1.58	79.75%	2.73	68.50%
FE (SF 1.0%)	10.32	75.19%	0.15	53.33%	15.10	68.68%	0.30	-6.67%	1.10	21.82%
FE (SF 1.5%)	11.47	77.68%	0.26	73.08%	17.30	72.66%	0.40	20.00%	1.23	30.08%
FE (SF 2.0%)	12.65	79.76%	0.09	22.22%	20.70	77.15%	0.46	30.43%	1.09	21.10%
FE (SF 2.5%)	19.72	87.02%	0.30	76.67%	25.40	81.38%	0.50	36.00%	1.11	22.52%
FE (SF 3.0%)	21.87	88.29%	0.41	82.93%	28.60	83.46%	0.55	41.82%	1.26	31.75%

It can be concluded that the use of the different types of fiber assisted in enhancing the structural performance of these beams. Furthermore, the response of the beam specimen reinforced with aramid fibers, FE (AF) outperformed the other beam specimens in terms of load levels, while, the beam reinforced with PVA fibers, FE (PVA) showed higher deflection levels.

4.2 Fiber volume fraction

Five different fibers' volume fractions have been employed to investigate the effect of fiber volume fractions on the behavior of fiber reinforced concrete beams. It is noteworthy that the geometrical properties of developed FE models are similar to those used in the experimental study

of Jun Zhang *et al.* (Zhang, Wang *et al.* 2014). The investigated fibers' volume fractions are 1, 1.5, 2, 2.5 and 3% for each fiber type. Thus, twenty-five new FE models are developed representing concrete beams reinforced with polyvinyl alcohol (PVA), aramid (AF), glass (GF), basalt (BF), and steel (SF) fibers, respectively. Fig. 8 shows the load–deflection response of the developed models, as well as Table 6 provides the deflection and load-carrying capacity at cracking and failure of the studied beams. It is obvious from Fig. 8 and Table 6 that there is a clear correlation between the volume fraction of the fibers and load-carrying capacity of these beams. As expected, the load-carrying capacity of each beam tends to increase using higher volume fraction. The increase can be attributed to the bridging action of the fibers across the cracks which restrained the propagation of micro cracks at the inception only. The stress is transferred to the bridging fibers after the flexural failure, which contains the crack propagation for some time and thus tensile strength is enhanced (Patel, Desai *et al.* 2012, Jiang, Fan *et al.* 2014).

It is evident from Fig. 8 that fiber addition had a beneficial effect on the load-carrying capacity of fiber reinforced concrete beams when compared with plain concrete and is in harmony with the finding of other researchers (Song and Hwang 2004, Sivakumar and Santhanam 2007, Kizilkanat, Kabay *et al.* 2015). However, the enhancement in load-carrying capacity was more prominent for beams reinforced with aramid fiber (AF) when compared to other fibers. The slopes of the pre-peak region in the load-carrying capacity response were similar irrespective of the fiber. However, the peak loads sustained by the concrete beams were found to be dependent on the fiber type and dosage. In fact, the load-carrying capacity of beams reinforced with polyvinyl alcohol (PVA), aramid (AF), glass (GF), basalt (BF), and steel (SF) fibers at fiber dosage 3% increased by (69.99%), (84.55%), (78.25%), (81.40%), and (83.46%), respectively over that of the reference specimen (PC). Furthermore, the ductility of the beam specimens reinforced with higher fiber volume fraction was increased as indicated in Fig. 8 and Table 6. Indeed, the ductility of FE (PVA 3%), FE (AF 3%), FE (GF 3%), FE (BF 3%), and FE (SF 3%) models was increased by (94.42%), (64.44%), (89.19%), (79.75%), and (41.82%), respectively over that of the reference specimen (PC). It could be concluded that using short fiber materials as internal reinforcement led to enhance the load-carrying capacity of structural concrete members with high ductility behavior.

4.3 Concrete compressive strength

The effect of the concrete compressive strength on the behavior of concrete beams reinforced with polyvinyl alcohol (PVA), aramid (AF), glass (GF), basalt (BF), and steel (SF) fibers has been studied. Ten additional FE models were developed with concrete compressive strengths of 45 and 65 MPa and designated as FE (PVA 45 MPa), FE (PVA 65 MPa), FE (AF 45 MPa), FE (AF 65 MPa), FE (GF 45 MPa), FE (GF 65 MPa), FE (BF 45 MPa), FE (BF 65 MPa), FE (SF 45 MPa), and FE (SF 65 MPa), respectively. The additional FE models were developed having the same geometrical properties used in the specimen EXP (PVA). The results of the developed models are compared with specimens FE (PVA), FE (AF), FE (GF), FE (BF), and FE (SF), respectively that had a compressive strength of 30 MPa. The results of the load–deflection curves of these beams are shown in Fig. 9. Table 7 provides the results of the ultimate load in the developed models along with the associated mid-span deflection at failure. It can be seen from Fig. 9 and Table 7 that the models of (65 MPa) compressive strength achieved a higher load-carrying capacity than that of (30 MPa) compressive strength models by (18.78%), (16.35%), (14.28%), (14.10%), and (19.98%) along with a decrease of (57.32%), (35.71%), (9.63%), (23.91%), and (43.75%) in the associated mid-span deflection for beams reinforced with PVA, AF, GF, BF, and SF, respectively. However,

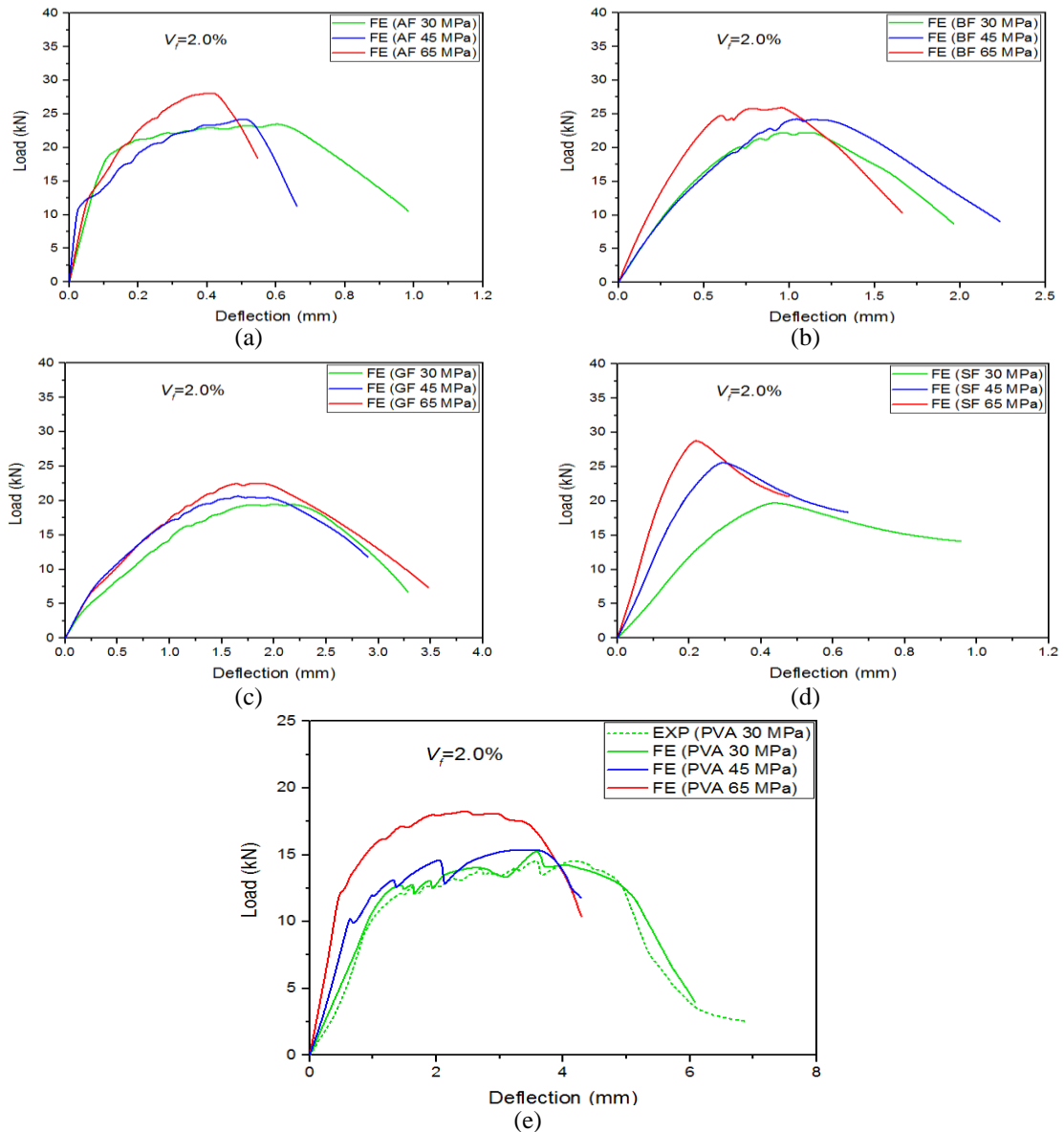


Fig. 9 Effect of concrete compressive strength on the response of fiber reinforced concrete beams

the models of (45 MPa) compressive strength experienced a slight increment in the ultimate load compared to that of (30 MPa) compressive strength models as shown in Fig. 9 and Table 7.

4.4 Crack patterns

The numerical cracking patterns at failure for the beams reinforced with polyvinyl alcohol (PVA), aramid (AF), glass (GF), basalt (BF), and steel (SF) fibers at 3% fiber volume fraction are presented in Fig. 10. Generally, for all the beams, the cracks were almost vertical in the bending

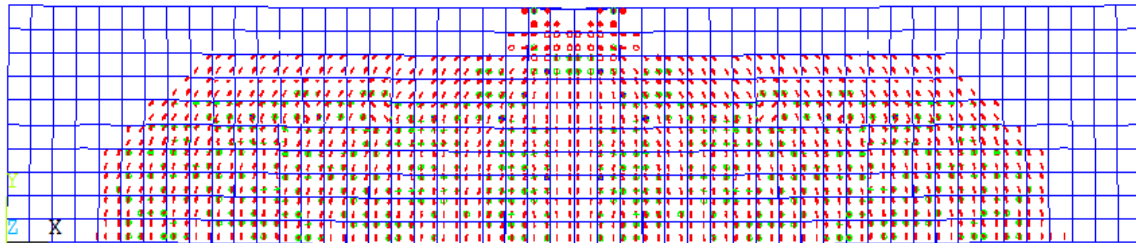
Table 7 Effect of concrete compressive strength

Specimen	Cracking load (kN)	% Difference (FE/FE 30 MPa)	Cracking deflection (mm)	% Difference (FE/FE 30 MPa)	Ultimate load (kN)	% Difference (FE/FE 30 MPa)	Ultimate deflection (mm)	% Difference (FE/FE 30 MPa)	Failure deflection (mm)	% Difference (FE/FE 30 MPa)
FE (PVA 30 MPa)	12.52	-----	1.68	-----	14.92	-----	3.87	-----	6.98	-----
FE (PVA 45 MPa)	13.28	5.72%	1.76	4.55%	15.31	2.55%	3.26	-18.71%	4.20	-66.19%
FE (PVA 65 MPa)	16.54	24.30%	1.08	-55.56%	18.37	18.78%	2.46	-57.32%	4.10	-70.24%
FE (AF 30 MPa)	15.45	-----	0.11	-----	23.63	-----	0.57	-----	1.08	-----
FE (AF 45 MPa)	19.76	21.81%	0.23	52.17%	24.26	2.60%	0.51	-11.76%	0.66	-63.64%
FE (AF 65 MPa)	23.21	33.43%	0.20	45.00%	28.25	16.35%	0.42	-35.71%	0.56	-92.86%
FE (GF 30 MPa)	14.87	-----	1.07	-----	19.51	-----	2.05	-----	3.36	-----
FE (GF 45 MPa)	17.38	14.44%	1.02	-4.90%	20.45	4.60%	1.97	-4.06%	2.88	-16.67%
FE (GF 65 MPa)	19.61	24.17%	1.23	13.01%	22.76	14.28%	1.87	-9.63%	3.51	4.27%
FE (BF 30 MPa)	14.53	-----	0.68	-----	22.42	-----	1.14	-----	2.01	-----
FE (BF 45 MPa)	19.01	23.57%	0.69	1.45%	24.38	8.04%	1.07	-6.54%	2.25	10.67%
FE (BF 65 MPa)	21.47	32.32%	0.42	-61.90%	26.10	14.10%	0.92	-23.91%	1.68	-19.64%
FE (SF 30 MPa)	12.65	-----	0.09	-----	20.70	-----	0.46	-----	1.09	-----
FE (SF 45 MPa)	14.96	15.44%	0.13	30.77%	21.00	1.43%	0.40	-15.00%	0.68	-60.29%
FE (SF 65 MPa)	18.38	31.18%	0.11	18.18%	25.87	19.98%	0.32	-43.75%	0.50	-118.00%

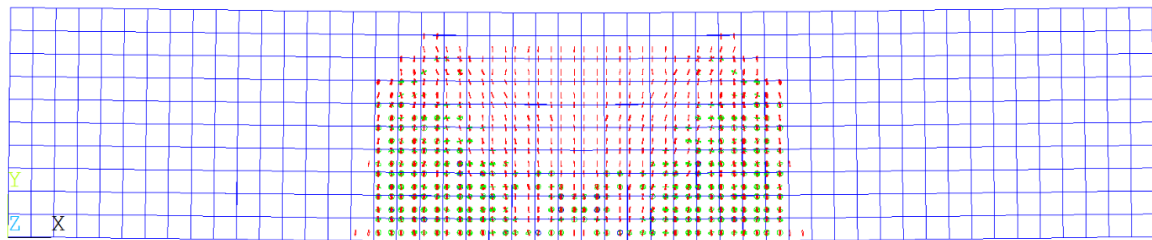
span while, inclined in the shear region.

It can be observed that the beams reinforced with polyvinyl alcohol (PVA) fibers show a greater number of cracks than the other beams. This result is probably due to the mechanical and physical properties of PVA fibers that provide a more widespread cracking. Consequently, the dissipated energy at failure was higher for the beams reinforced with PVA fibers at (30) MPa compressive strength. It can be seen that the cracks in the beams grow symmetrically on both sides of the beam due to the beam geometry, boundary and loading conditions are all symmetric. Also, this could be attributed to the uniform distribution and orientation of the fibers (Wille and Parra-Montesinos 2012), which adopted in this study by using homogenous models.

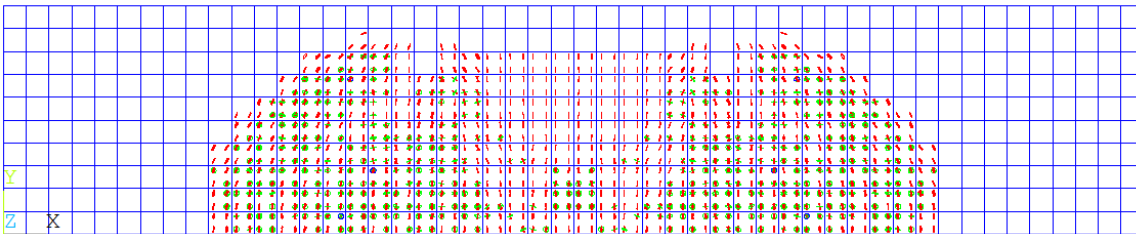
As illustrated in Fig. 10, the beams underwent three stages (refer (Weibull 1939, Weibull 1951, Rossi, Arca *et al.* 2005, Magureanu, Sosa *et al.* 2012)). The first was linear-elastic stage, where both matrix and fibers behaved elastically. The maximum flexural strength attained in this stage



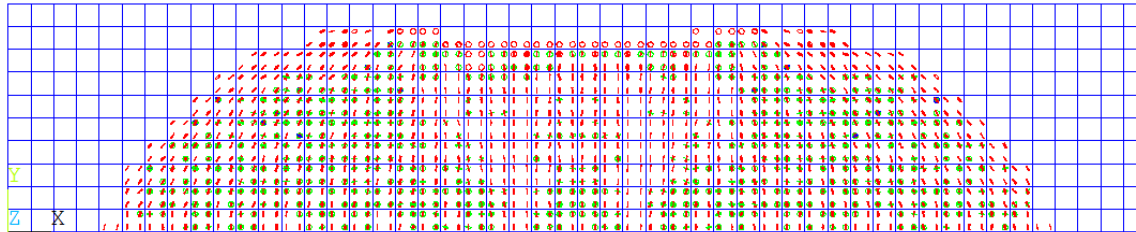
(a) Concrete beam reinforced with PVA fibers



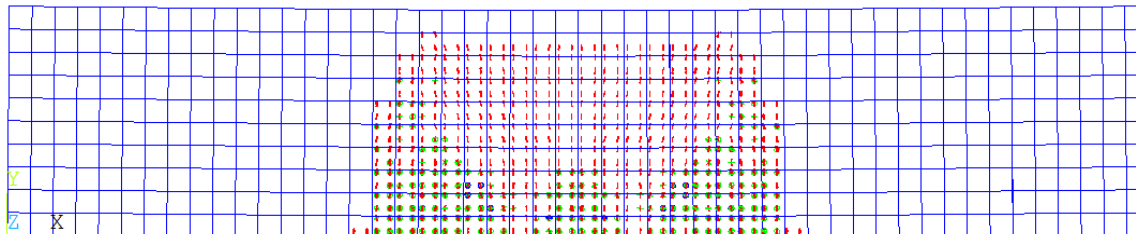
(a) Concrete beam reinforced with AF fibers



(b) Concrete beam reinforced with BF fibers



(c) Concrete beam reinforced with GF fibers



(d) Concrete beam reinforced with SF fibers

Fig. 10 Numerical cracking patterns for the beams reinforced with polyvinyl alcohol (PVA), aramid (AF), glass (GF), basalt (BF), and steel (SF) fibers at 3% fiber volume fraction

corresponded to the matrix strength while the fiber contributed little to the overall structural

behavior. The next stage followed by the appearance of micro-cracks near the loading supports where the matrix cracking strain was exceeded. As the load increased, the micro-cracks merged into a single macro-crack. The crack surfaces were bridged by closely spaced fibers. Due to the high strength of the fibers and strong bond between the fibers and the matrix, the macro-crack widens slowly in this stage, leading to certain level of strain hardening. This strain hardening behavior distinguishes fiber reinforced concrete beams from conventional types of concrete. This stage is called pseudo-strain hardening stage. After a considerable deflection, where the fibers were no longer capable of sustaining the maximum tensile stress, due to the increase in crack width of the structure, the final stage of the beam specimens occurred as a single macro-crack localized in the structure section. This stage is called the descending region (softening region). Similar to the previous stage, this region is very pronounced for fiber reinforced concrete beams and it is controlled by fiber pull-out across the concrete crack and fiber pull-out depends on the type and length of the fiber. The deformation behavior in this stage is related to half the length of the fiber, 6 mm in this study. Furthermore, it was also observed that the load increased at a very small rate in pseudo-strain hardening phase compared with the elastic phase, and high deformation took place with reduced modulus of elasticity. Further details of these stages are explained in (Hassan, Jones *et al.* 2012).

5. Conclusions

A total of thirty-eight 3D nonlinear FE models were developed in the present investigation to simulate the response of concrete beams reinforced with a synthetic, mineral, and conventional steel fibers. Four models were utilized to validate the accuracy of the results by comparing the predicted load versus mid-span deflection response values with the experimental results obtained from an available literature. The remaining thirty-four models were used to study numerically the effect of fiber reinforcement material type, fiber volume fraction, and concrete compressive strength on the behavior of the reinforced concrete beam specimens. Furthermore, the numerical cracking patterns at failure for the beams reinforced with different type of fibers were investigated. The main finding can be summarized as follow:

- The developed FE models predicted accurately the load–deflection capacity of the experimental specimens with a deviation less than 10%.
- The developed FE models, with an approach grounded on the solid basis of micromechanics, capable to be employed by researchers and engineers as a numerical tool to investigate the behavior of concrete beams reinforced with different types of fibers at macroscale and microscale.
- The use of different material types of fibers yielded different responses of the beam specimens. Regarding maximum load levels, the response of the beam specimen reinforced with aramid (AF) fibers outperformed the other beams that were reinforced with polyvinyl alcohol (PVA), glass (GF), basalt (BF), and steel (SF) fibers.
- The load-carrying capacity of the beams reinforced with aramid polyvinyl alcohol (PVA), (AF), glass (GF), basalt (BF), and steel (SF) fibers at 3% fiber volume fraction increased by (84.55%), (78.25%), (81.40%), and (83.46%), respectively over that of the reference specimen (PC).
- The ductility of the beams reinforced with aramid (AF), glass (GF), basalt (BF), and steel (SF) fibers at 3% fiber volume fraction increased by (69.99%), (64.44%), (89.19%), (79.75%), and (41.82%), respectively over that of the reference specimen (PC).

- The models of (65 MPa) compressive strength achieved a higher load-carrying capacity than that of (30 MPa) compressive strength models along with a decrease in the associated mid-span deflection for beams reinforced with different type of fibers.
- For all the beams, the cracks were almost vertical in the bending span and inclined in the shear region. Furthermore, the beams reinforced with polyvinyl alcohol (PVA) fibers show greater number of cracks than the other beams.

Acknowledgements

The researchers gratefully acknowledge the technical support provided by Faculty of Civil Engineering at University of Gaziantep.

References

- ANSYS - Release Version 16. (2015), "A finite element computer software and user manual for nonlinear structural analysis".
- Bencardino, F., Condello, A. and Ombres, L. (2016), "Numerical and analytical modeling of concrete beams with steel, FRP and hybrid FRP-steel reinforcements", *Compos. Struct.*, **140**, 53-65.
- Daniel, I.M., Ishai, O., Daniel, I.M. and Daniel, I. (1994), *Engineering mechanics of composite materials*, **3**, New York, Oxford university press.
- Di Maida, P., Radi, E., Sciancalepore, C. and Bondioli, F. (2015), "Pullout behavior of polypropylene macro-synthetic fibers treated with nano-silica", *Constr. Build. Mater.*, **82**, 39-44.
- Hannawi, K., Bian, H., Prince-Agbodjan, W. and Raghavan, B. (2016), "Effect of different types of fibers on the microstructure and the mechanical behavior of Ultra-High Performance Fiber-Reinforced Concretes", *Compos. Part B: Eng.*, **86**, 214-220.
- Hassan, A.M.T., Jones, S.W. and Mahmud, G.H. (2012), "Experimental test methods to determine the uniaxial tensile and compressive behaviour of ultra high performance fibre reinforced concrete (UHPFRC)", *Constr. Build. Mater.*, **37**, 874-882.
- Hawileh, R. (2015), "Finite element modeling of reinforced concrete beams with a hybrid combination of steel and aramid reinforcement", *Mater. Des.*, **65**, 831-839.
- Hawileh, R.A., El-Maaddawy, T.A. and Naser, M.Z. (2012), "Nonlinear finite element modeling of concrete deep beams with openings strengthened with externally-bonded composites", *Mater. Des.*, **42**, 378-387.
- Hawileh, R.A., Naser, M.Z. and Abdalla, J.A. (2013), "Finite element simulation of reinforced concrete beams externally strengthened with short-length CFRP plates", *Compos. Part B: Eng.*, **45**(1), 1722-1730.
- Hognestad, E., Hanson, N.W. and McHenry, D. (1955), "Concrete stress distribution in ultimate strength design", *J. Proceedings*, **52**(12), 455-480.
- Jiang, C., Fan, K., Wu, F. and Chen, D. (2014), "Experimental study on the mechanical properties and microstructure of chopped basalt fibre reinforced concrete", *Mater. Des.*, **58**, 187-193.
- Kanda, T., Lin, Z. and Li, V.C. (2000), "Tensile stress-strain modeling of pseudostrain hardening cementitious composites", *J. Mater. Civil Eng.*, **12**(2), 147-156.
- Kizilkanat, A.B., Kabay, N., Akyüncü, V., Chowdhury, S. and Akça, A.H. (2015), "Mechanical properties and fracture behavior of basalt and glass fiber reinforced concrete: An experimental study", *Constr. Build. Mater.*, **100**, 218-224.
- Li, F. (1998), *Fracture characterization of fiber reinforced concrete in direct uniaxial tension*.
- Lu, X. and Hsu, C.T.T. (2006), "Behavior of high strength concrete with and without steel fiber reinforcement in triaxial compression", *Cement Concrete Res.*, **36**(9), 1679-1685.
- Maalej, M. and Leong, K.S. (2005), "Engineered cementitious composites for effective FRP-strengthening

- of RC beams”, *Compos. Sci. Tech.*, **65**(7), 1120-1128.
- Magureanu, C., Sosa, I., Negrutiu, C. and Heghes, B. (2012), “Mechanical properties and durability of ultra-high-performance concrete”, *ACI Mater. J.*, **109**(2).
- Mahmud, G.H., Yang, Z. and Hassan, A.M. (2013), “Experimental and numerical studies of size effects of Ultra High Performance Steel Fibre Reinforced Concrete (UHPRFC) beams”, *Constr. Build. Mater.*, **48**, 1027-1034.
- Manos, G.C., Theofanous, M. and Katakalos, K. (2014), “Numerical simulation of the shear behaviour of reinforced concrete rectangular beam specimens with or without FRP-strip shear reinforcement”, *Adv. Eng. Softw.*, **67**, 47-56.
- Markovic, I. (2006), “High-performance hybrid-fibre concrete: development and utilisation”, TU Delft, Delft University of Technology.
- Marshall, I. (1992), *Fibre reinforced cements and concretes: Recent developments*, Edited by RN Swamy and B. Barr. Elsevier Science Publishers, London, Elsevier.
- Monteiro, P. (2006), *Concrete: microstructure, properties, and materials*, McGraw-Hill Publishing.
- Nagaraj, T.S. and Dwarakanath, H.V. (1984), “Structural response of partially fibrous concrete beams”, *J. Struct. Eng.*, **110**(11), 2798-2812.
- Nataraja, M.C., Dhang, N. and Gupta, A.P. (1999), “Stress-strain curves for steel-fiber reinforced concrete under compression”, *Cement Concrete Compos.*, **21**(5), 383-390.
- Nguyen, D.L., Ryu, G.S., Koh, K.T. and Kim, D.J. (2014), “Size and geometry dependent tensile behavior of ultra-high-performance fiber-reinforced concrete”, *Compos. Part B: Eng.*, **58**, 279-292.
- Patel, P.A., Desai, A.K. and Desai, K.A. (2012), “Evaluation of engineering properties for polypropylene fiber reinforced concrete”, *Int. J. Adv. Eng. Tech.*, **3**(1), 42-45.
- Rossi, P., Arca, A., Parant, E. and Fakhri, P. (2005), “Bending and compressive behaviours of a new cement composite”, *Cement Concrete Res.*, **35**(1), 27-33.
- Sivakumar, A. and Santhanam, M. (2007), “Mechanical properties of high strength concrete reinforced with metallic and non-metallic fibres”, *Cement Concrete Compos.*, **29**(8), 603-608.
- Song, P.S. and Hwang, S. (2004), “Mechanical properties of high-strength steel fiber-reinforced concrete”, *Constr. Build. Mater.*, **18**(9), 669-673.
- Vasiliev, V.V. and Morozov, E. (2013), *Advanced mechanics of composite materials and structural elements*, Newnes.
- Weibull, W. (1939), *A statistical theory of the strength of materials*, Generalstabens litografiska anstalts förlag.
- Weibull, W. (1951), “A statistical distribution function of wide applicability”, *J. Appl. Mech.*, **18**, 293.
- Willam, K. and Warnke, E. (1975), “Constitutive model for the triaxial behavior of concrete”, *Proceedings of the international association for bridge and structural engineering*, ISMES, Bergamo, Italy.
- Wille, K., El-Tawil, S. and Naaman, A.E. (2014), “Properties of strain hardening ultra high performance fiber reinforced concrete (UHP-FRC) under direct tensile loading”, *Cement Concrete Compos.*, **48**, 53-66.
- Wille, K. and Parra-Montesinos, G.J. (2012), “Effect of beam size, casting method, and support conditions on flexural behavior of Ultra-High-Performance fiber-reinforced concrete”, *ACI Mater. J.*, **109**(3).
- Yoo, D.Y., Yoon, Y.S. and Banthia, N. (2015), “Predicting the post-cracking behavior of normal-and high-strength steel-fiber-reinforced concrete beams”, *Constr. Build. Mater.*, **93**, 477-485.